

The effect of Reynolds number on boundary layer turbulence

David B. DeGraaff^{a,*}, Donald R. Webster^b, John K. Eaton^a

^a Department of Mechanical Engineering, Stanford University, Bldg. 500, Rm. 501E, Stanford, CA 94305-3030, USA

^b School of Civil and Environmental Engineering, Georgia Institute of Technology, 790 Atlantic Drive, Atlanta, GA 30332-0355, USA

Received 13 February 1998; received in revised form 29 June 1998; accepted 11 September 1998

Abstract

A new facility for studying high Reynolds number incompressible turbulent boundary layer flows has been constructed. It consists of a moderately sized wind tunnel, completely enclosed by a pressure vessel, which can raise the ambient air pressure in and around the wind tunnel to 8 atmospheres. This results in a Reynolds number range of about 20:1, while maintaining incompressible flow. Results are presented for the zero pressure gradient flat plate boundary layer over a momentum thickness Reynolds number range 1500–15 000. Scaling issues for high Reynolds number non-equilibrium boundary layers are discussed, with data comparing the three-dimensional turbulent boundary layer flow over a swept bump at Reynolds numbers of 3800 and 8600. It is found that successful prediction of these types of flows must include length scales which do not scale on Reynolds number, but are inherent to the geometry of the flow. © 1999 Elsevier Science Inc. All rights reserved.

Keywords: Reynolds number; Turbulent boundary layer

1. Introduction

It has long been assumed that boundary layer turbulence approaches an asymptotic state for momentum thickness Reynolds numbers above 6000. This has led to the incorporation of dimensionless structure parameters measured at relatively low Reynolds numbers into turbulence models which are then used to predict much higher Reynolds number flows. For example, the constants in turbulence models are generally tuned to match low Reynolds number experimental data because of its high resolution, or low Reynolds number numerical data bases from Spalart [1] or Kim et al. [2] because of the detailed information available.

Because the dominant flow structures in the inner and outer layers of the boundary layer are so different, it is likely that there are significant Reynolds number effects on the dimensionless structural parameters. The inner region is dominated by long streamwise low-speed streaks and longitudinal vortices, which scale on the viscous length scale (ν/U_τ). The outer region contains more three-dimensional structures often characterized as hairpin vortices, which scale on outer length scales,

such as the boundary layer thickness [3]. Since the viscous length scale decreases rapidly with Reynolds number, and the outer length scales are only a weak function of Reynolds number, the inner and outer scales become increasingly disparate with increasing Reynolds number. For example, at a momentum thickness Reynolds number of 1000, the region below $y^+ = 100$ occupies approximately 14% of the total boundary layer thickness, and accounts for almost all of the turbulence production. At a Reynolds number of 6000, this region occupies only about 4% of the total boundary layer thickness and still accounts for a large fraction of the total turbulence production. However, at a Reynolds number of 20 000, the region below $y^+ = 100$ occupies only about 1.5% of the boundary layer thickness, and accounts for only a small fraction of the total turbulence production. It therefore seems appropriate to examine high Reynolds number turbulent boundary layers in the same detail as we have studied lower Reynolds number flows to determine if the models we are presently using are really capable of accurately predicting high Reynolds number flows.

Several recent studies have provided high Reynolds number data for the canonical flat plate zero pressure gradient boundary layer [4–6]. These data collapse well in traditional inner/outer scaling with the appropriate scaling variables in the inner region being the skin fric-

* Corresponding author. Tel.: 1 650 723 8481; fax: 1 650 723 4548; e-mail: degraaff@stanford.edu

tion and the kinematic viscosity, and the outer layer scale being dictated by the boundary layer thickness and the wake velocity deficit. These scaling parameters are simple known functions of only the Reynolds number [7], and extrapolation of the existing behavior from low and moderate Reynolds number experiments to much higher Reynolds numbers thus appears to be appropriate.

More complex turbulent flows, however, are often not well described by the Reynolds number alone. These non-equilibrium flows have additional length or time scales introduced by the geometry or dynamics of the system. For example, a rapid change in wall curvature, pressure gradient, or wall roughness causes the formation of an internal layer. This layer is in equilibrium with the boundary condition at the wall, and then evolves outward to eventually bring the rest of the boundary layer into equilibrium with the modified boundary condition. The distance from the wall to the interface between the internal layer and outer boundary layer provides an additional length scale that is not a simple function of the Reynolds number.

A geometric length scale is important in most separated flows and particularly in the flow over a step or cavity where the geometric scale dominates the flow development. Such a scale does not change with Reynolds number while the length scale of near-wall structures in the same flow changes rapidly. The interaction of the near-wall structures with large vortices formed in the separated flow thus would be expected to be dependent on the Reynolds number.

The introduction of a spanwise pressure gradient or wall shear causes a two-dimensional boundary layer to become three-dimensional with a mean cross flow relative to the free stream direction. This introduces another length scale, namely the height of the peak in the cross flow profile. At low Reynolds number this peak may occur as low as y^+ of 20, meaning that the cross flow has a strong interaction with near-wall structure. At high Reynolds numbers, the peak is much farther from the wall when measured in inner coordinates [8].

It is clear that non-equilibrium turbulent flows have additional length and/or time scales that must be considered. These scales do not evolve with Reynolds number in the same way as the traditional inner and outer scales. One might guess then that the dimensionless structure parameters might continue to change in non-equilibrium flows up to very high Reynolds number.

The objective of the present work is to examine the effects of varying Reynolds numbers on non-equilibrium turbulent boundary layers. A new facility was constructed allowing a wide variation in Reynolds number in a flexible, moderate scale wind tunnel. As a test of the facility, and to corroborate previous data, two-dimensional boundary layer data are presented for Reynolds numbers ranging from 1500 to 15 000. The effects of Reynolds number on a non-equilibrium boundary layer developing over a swept bump are also examined.

2. Experimental apparatus and techniques

The experiments were performed in the tunnel floor boundary layer of a wind tunnel which is completely enclosed in a pressure vessel as shown in Fig. 1. This facility provides a wide Reynolds number range by regulating the ambient pressure from one to eight atmospheres. In this approach, the tunnel walls need only support the dynamic pressure loads of the flow and not the absolute pressure. Thus, typical construction materials for atmospheric pressure wind tunnels can be used, and the tunnel can be modified easily for visual or probe access. A total Reynolds number range of approximately 20 : 1 is possible by varying both the flow speed and density. Additionally, the flow maintains a low Mach number (approximately 0.04), and can therefore be modeled as incompressible.

The closed circuit wind tunnel was designed with a very short flow conditioning section and uses the curved door of the pressure vessel as a turning duct, in order to maximize the test section length. The test section is 2.9 m long, with a 150 by 710 mm rectangular test section. The nominal operating velocity is 15 m/s, with a free stream turbulence level of 0.2%.

Velocity measurements were performed with the single-wire and cross-wire probes described in Littell and Eaton [9]. The probes were strung with 2.5 μm platinum-coated tungsten wire which was copper plated and etched for an active length to diameter ratio of 250. The spacing between the cross-wires was 0.35 mm. The probes were connected to TSI constant temperature anemometers (model IFA-100), operating with a resistance overheat ratio of 1.8. The effective wire angles were found using a yawing procedure described in Westphal and Mehta [10]. The probes were positioned using a two axis traverse, and zeroed by contact with the conducting floor of the test section. Data acquisition was performed with a 486 PC clone and National Instruments AT-MIO-16 and GPIB-PCII boards. An external simultaneous sample and hold circuit was used to collect cross-wire voltages. Further details of the operation of these probes can be found in Webster et al. [11]. The mean velocity uncertainty is estimated to be 3% of the streamwise velocity, the normal stress uncertainty is 5% of the local value of $\overline{u'u'}$, and the shear stress mea-

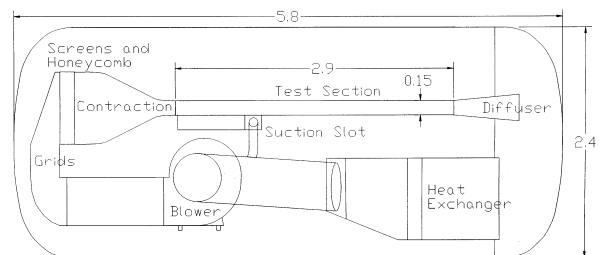


Fig. 1. Wind tunnel schematic. Outer shell is the pressure vessel. All dimensions are in meters.

measurements have an uncertainty of 10% of the local value of $\overline{u'v'}$.

This paper presents data from two different experimental setups. The first is flat plate data from the test section floor. The second is the perturbed boundary layer flow over a bump swept at 45° with respect to the freestream velocity vector. The bump shape is described by three tangential circular arcs, and is illustrated in Fig. 2. The initial boundary layer thickness to bump height ratio was 1.5, and the boundary layer thickness to convex radius of curvature was 0.06. The boundary layer originates at a suction slot which is swept parallel to the leading edge of the bump. A parallel boundary layer trip insures that the boundary layer is uniform along lines parallel to the bump. Mean velocity and skin friction measurements showed excellent uniformity across the span so only centerline measurements are reported here. All measurements are reported in the coordinate system shown on Fig. 2, with x , y , and z , being the streamwise, wall normal, and spanwise directions, respectively. The y -axis is maintained normal to the flat plate tunnel floor, with its origin on the tunnel floor or the bump surface.

3. Results and discussion

3.1. The flat plate

Fig. 3 shows mean streamwise velocity measurements on a flat plate for Reynolds numbers from 1500 to 15 000, plotted in inner coordinates, and Fig. 4 shows the same data plotted in outer coordinates. For the lower two Reynolds numbers, data extend into the sub layer, while only the log region is attained for the higher Reynolds numbers. The inner layer collapses very well on the standard log law of the wall. This is perhaps not surprising since the wall velocity used in scaling the plots was derived by fitting the data to the log law. As many investigators have noted previously, the length of the log

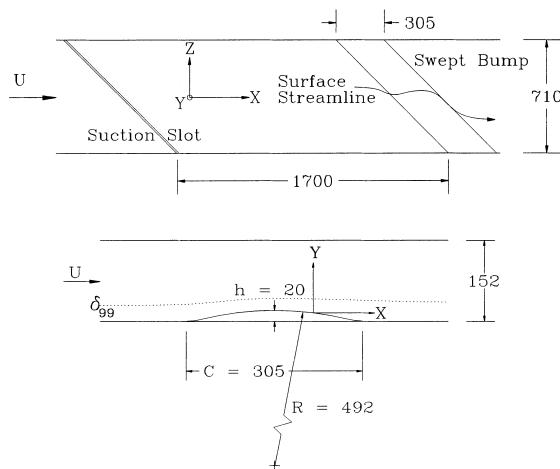


Fig. 2. Top view of test section, and side view of bump. All dimensions are in millimeters.

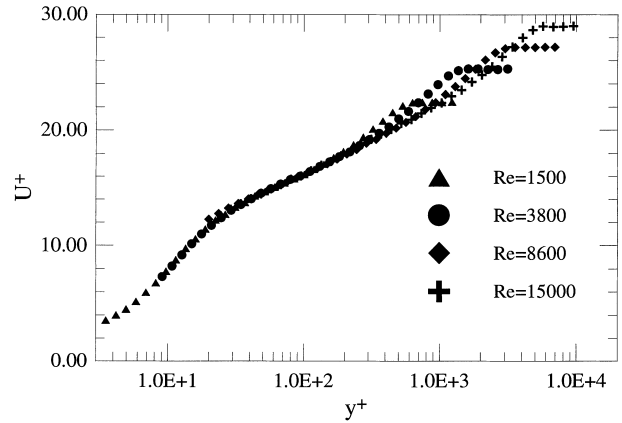


Fig. 3. Mean streamwise velocity profiles at different momentum thickness Reynolds numbers: inner coordinates.

law region increases in viscous units with increasing Reynolds number, and the magnitude of the wake decreases. The data agree well with data compiled by Fernholz and Finley [6] in their extensive review of incompressible zero pressure gradient turbulent boundary layers.

Fig. 4 shows good collapse of the data in the outer region. Note that the outer region occupies a much larger fraction of the boundary thickness at high Reynolds number.

Fig. 5 shows the streamwise normal stresses plotted in inner coordinates. For the lower Reynolds number cases, the near-wall peak is resolved. The data collapse at the near wall peak at y^+ of 12–15, with a magnitude of approximately 7.3. The higher Reynolds number hot-wire measurements clearly show the effects of poor measurement resolution near the wall, as they are not collapsing on the same near-wall peak with the lower two Reynolds number cases. Mochizuki et al. [12] compiled 47 near-wall data sets which demonstrate the peak height is Reynolds number independent, and the

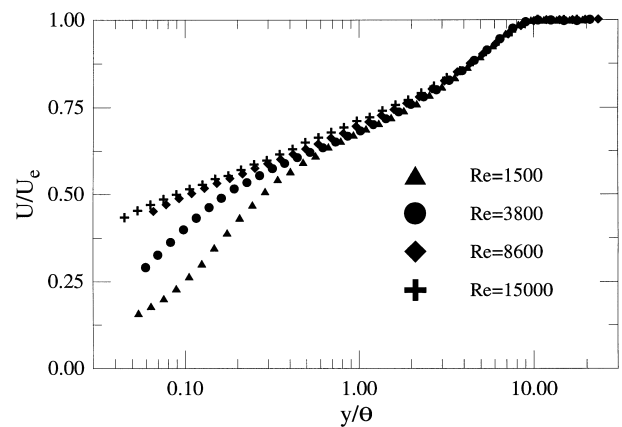


Fig. 4. Mean streamwise velocity profiles at different momentum thickness Reynolds numbers: outer coordinates.

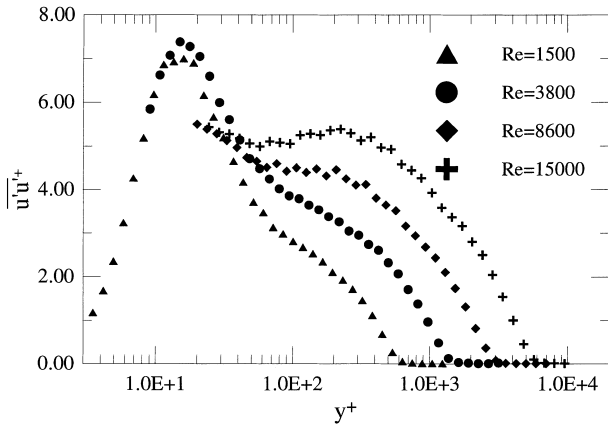


Fig. 5. Streamwise normal stress profiles at different momentum thickness Reynolds numbers: inner coordinates.

distance of the peak from the wall in viscous lengths is a very weak function of Reynolds number.

Resolution of the turbulence is a fundamental problem for most high Reynolds number experiments. In this study the near-wall turbulence data are only well resolved for the lower two Reynolds number cases, since the length of the hot wire in viscous units is 4, 11, 25, and 45 for Reynolds numbers of 1500, 3800, 8600, and 15 000, respectively.

Fig. 6 shows the streamwise normal stress in outer coordinates, which collapses fairly well for y/θ larger than one. It can be seen that the increasing magnitude of $\overline{u'u}$ for $y^+ > 100$ with increasing Reynolds number shown in Fig. 5 is an artifact of the inner scaling. The present data both corroborate the previous measurements and serve as a check on our facility. As a further check, we repeated one Reynolds number case by raising the ambient pressure, and compensating by reducing the freestream velocity. The dimensionless data were identical for the two cases.

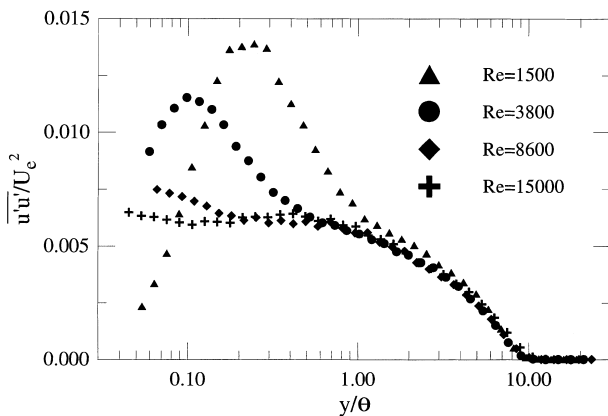


Fig. 6. Streamwise normal stress profiles at different momentum thickness Reynolds numbers: outer coordinates.

3.2. The swept bump

In order to study non-equilibrium effects, a swept bump was installed on the test section floor as shown in Fig. 2. The flow over the bump is subjected first to a short length of concave curvature with a mildly adverse pressure gradient, then a long convex curvature over the top of the bump, with a strongly favorable streamwise pressure gradient on the upstream side, followed by a strongly adverse streamwise pressure gradient on the downstream side of the bump. Finally, a short length of concave curvature and mild favorable pressure gradient at the rear of the bump brings the flow back to the flat test section floor downstream of the bump. The curvature and alternating signs of streamwise pressure gradient have a profound effect on the mean streamwise velocity. Profiles at different streamwise locations are shown in Fig. 7. The x' coordinate is the distance from the bump leading edge normalized by the bump cord. The incoming boundary layer is significantly thinned at the apex of the bump ($x' = 0.5$), and the log region is destroyed by the rapid acceleration. The boundary layer is thickest at the trailing edge of the bump ($x' = 1.0$), and then shows a rapid recovery. The last profile ($x' = 1.7$) is only 0.7 cord lengths behind the bump, and the profile lies almost on top of the incoming flat plate boundary layer profile ($x' = -0.5$). Flow visualization and shear stress measurements using an oil interferometry technique confirmed there was no separation on the back of the bump. Further details can be found in Webster et al. [13].

Because of the 45° sweep angle of the bump, spanwise pressure gradients caused significant skewing of the mean velocity vector near the wall. The top view of the test section in Fig. 2 shows the direction of shear stress near the wall with a surface streamline drawn on the bump. Along the leading edge of the bump, the spanwise flow is initially in the direction of the sweep of the bump, and then turns into the sweep as the flow goes over the bump apex. Along the trailing edge of the bump the

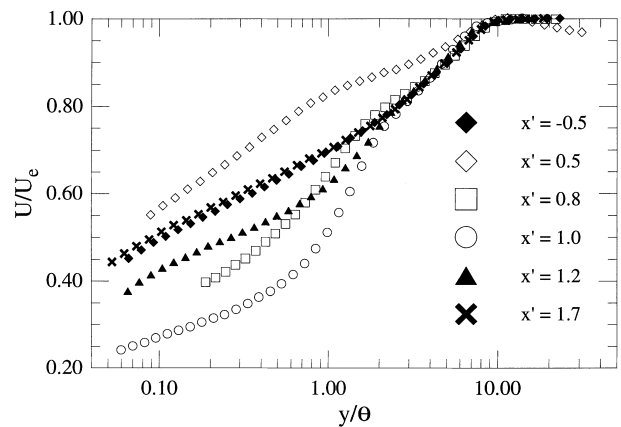


Fig. 7. Mean streamwise velocity profiles at different x -locations, for $Re_0 = 8600$.

shear stress vector is nearly parallel to the bump trailing edge, due to the combined effects of the spanwise pressure gradient, and deceleration of the flow from the adverse streamwise pressure gradient. This behavior is shown in inner coordinates in Fig. 8, for three streamwise locations. The profile at the apex has a negative near-wall peak, and the profile at the trailing edge has a large positive near-wall peak. The same data are plotted in Fig. 9, using the local freestream velocity and bump height for normalization. Clearly there is much better collapse of the data for the two Reynolds numbers. In this Reynolds number range, the height of the peak cross flow is a constant distance from the wall, independent of Reynolds number. Thus, the bump has introduced another length scale which is necessary to properly scale this flow.

Similar scaling arguments can be made based on the behavior of the shear stress behind the bump. Figs. 10 and 11 compare shear stress data taken at the trailing edge of the bump, for two different Reynolds numbers. Fig. 10 is in outer coordinates, and shows strong Reynolds number dependence on the peak shear stress when normalized by the local freestream velocity. Fig. 11 is in mixed coordinates, with the friction velocity normalizing the shear stress magnitude (an inner variable), and the bump height normalizing the distance from the wall (an outer variable). With this scaling the data collapse reasonably well. Note that in the log region, the shear stress normalized by the wall velocity is near unity for a standard two-dimensional turbulent boundary layer, where $\overline{u'v'}$ is the only shear stress. It is remarkable that in this highly perturbed flow, where $\overline{u'v'}$ is augmented by a factor of three, and the other Reynolds shear stresses are significant, the friction velocity is the appropriate scaling.

4. Conclusions

A unique facility for studying boundary layers over a wide range of Reynolds numbers has been developed. Measurements for a zero pressure gradient turbulent boundary layer agree well with standard log law and

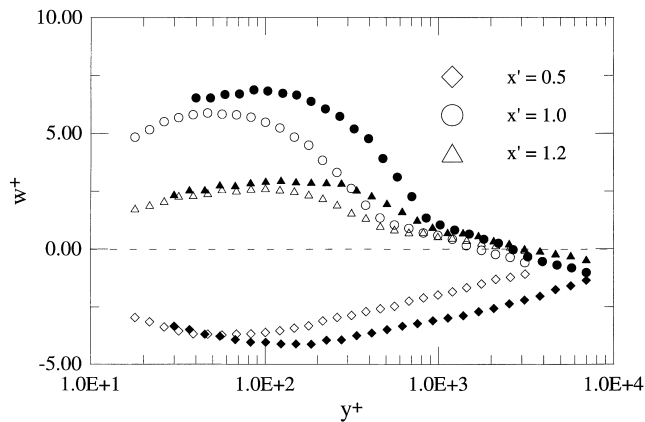


Fig. 8. Mean spanwise velocity profiles at different x -locations. Open symbols are $Re_\theta = 3800$, filled symbols are $Re_\theta = 8600$.

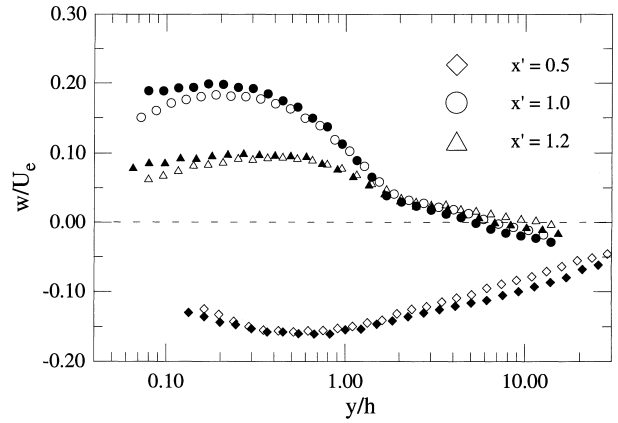


Fig. 9. Mean spanwise velocity profiles at different x -locations. Open symbols are $Re_\theta = 3800$, filled symbols are $Re_\theta = 8600$.

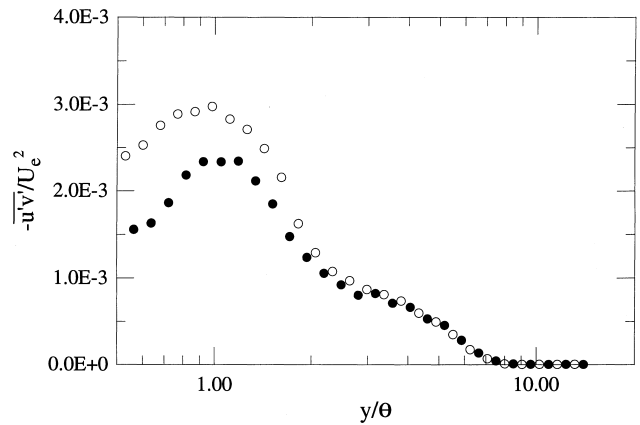


Fig. 10. Shear stress profiles at the bump trailing edge ($x' = 1.0$). Open symbols are $Re_\theta = 3800$, filled symbols are $Re_\theta = 8600$.

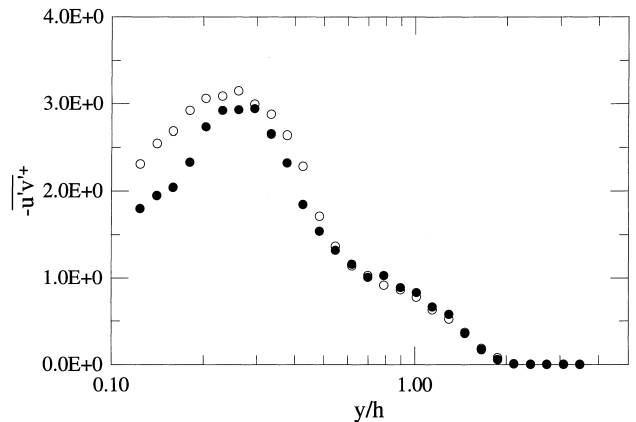


Fig. 11. Shear stress profiles at the bump trailing edge ($x' = 1.0$). Open symbols are $Re_\theta = 3800$, filled symbols are $Re_\theta = 8600$.

inner/outer scaling. This suggests that computations of these flows at Reynolds numbers significantly higher than those used to calibrate the turbulence models will be successful.

The three-dimensional turbulent boundary layer over a swept bump has been discussed with regard to scaling arguments. This is a typical non-equilibrium flow, in which new length scales are introduced by the geometry, which are necessary to scale both mean and turbulence quantities. It is clear that models which hope to accurately predict such flows need to include these additional scales.

5. Recommendations

Further investigation of the scaling issues in non-equilibrium flows requires turbulence measurements at higher Reynolds numbers. To acquire accurate measurements at high Reynolds numbers, the development of high resolution measurement systems is imperative.

Nomenclature

h	bump height, m
Re_θ	Reynolds number based on momentum thickness ($= U_e \theta / \nu$), dimensionless
U	streamwise velocity, m/s
U_e	local freestream velocity, m/s
U_τ	wall velocity ($= (\text{wall shear}/\text{fluid density})^{1/2}$), m/s
$\overline{u'u'}$	streamwise turbulent normal stress divided by fluid density, m^2/s^2
$\overline{u'v'}$	spanwise turbulent shear stress divided by fluid density, m^2/s^2
w	spanwise dimension, m
x'	distance to the leading edge of the bump, normalized by the bump cord length, dimensionless
y	wall normal direction, m
ν	dynamic viscosity, m^2/s
θ	boundary layer momentum thickness, m
+	indicates quantity has been nondimensionalized by inner variables: ν/U_τ for lengths, or U_τ for velocities

Acknowledgements

We gratefully acknowledge support of the Office of Naval Research under grant number N0001494-1-0070, monitored by Dr. L.P. Purtell.

References

- [1] P.R. Spalart, Direct Simulation of a Turbulent Boundary Layer up to $Re_\theta = 1410$, NASA Technical Memorandum No. TM-89407, 1986.
- [2] J. Kim, P. Moin, R.D. Moser, Turbulence statistics in fully-developed channel flow at low Reynolds number, *J. Fluid Mech.* 177 (1987) 133–166.
- [3] S.K. Robinson, Coherent motions in the turbulent boundary layer, *Annual Rev. Fluid Mech.* 23 (1991) 601–639.
- [4] W.S. Saric, Turbulent Boundary Layer In Subsonic and Supersonic Flow, AGARDograph No. 335, 1996.
- [5] M. Gad-el-Hak, P.R. Bandyopadhyay, Reynolds number effect in wall-bounded turbulent flows, *Appl. Mech. Rev.* 47 (8) (1994) 307–365.
- [6] H.H. Fernholz, P.J. Finley, The incompressible zero pressure gradient turbulent boundary layer: an assessment of the data, *Prog. Aerospace Sci.* 32 (1996) 245–311.
- [7] D.A. Coles, E.A. Hirst, The young person's guide to the data, AFOSR-IFP-Stanford Conference, vol. 2, 1968, pp. 1–19.
- [8] J.K. Eaton, Effects of mean flow three dimensionality on turbulent boundary-layer Structure, *AIAA J.* 33 (11) (1995) 2020–2025.
- [9] H.S. Littell, J.K. Eaton, Turbulence characteristics of the boundary layer on a rotating disk, *J. Fluid Mech.* 266 (1994) 175–207.
- [10] R.V. Westphal, R.D. Mehta, Crossed Hot-Wire Data Acquisition and Reduction System, NASA Technical Memorandum No. 85871, 1984.
- [11] D. Webster, D.B. DeGraaff, J.K. Eaton, Turbulent characteristics of a boundary layer over a two-dimensional bump, *J. Fluid Mech.* 320 (1996) 53–69.
- [12] S. Mochizuki, F.T.M. Nieuwstadt, Reynolds number dependence of the maximum in the streamwise velocity fluctuations in wall turbulence, *Exp. in Fluids* 21 (1996) 218–226.
- [13] D. Webster, D.B. DeGraaff, J.K. Eaton, Turbulent characteristics of a boundary layer over a swept bump, *J. Fluid Mech.* 323 (1996) 1–22.